42

HEIGHT-CORRELATION ANALYSIS OF DATA FROM AN S-BAND ZENITH-POINTING RADAR IN SINGAPORE

M. Thurai[1]*, V. N. Bringi[1], Y. H. Lee[2], L. S. Kumar[2], J. D. Eastment[3], and D. Ladd[3]

[1]Dept. of ECE, Colorado State University, Fort Collins, Colorado, USA
[2]School of Engineering, Nanyang Technological University, Singapore
[3]STFC Rutherford Appleton Laboratory, Chilton, Didcot, Oxon, UK

1, INTRODUCTION

Information on height correlation of radar reflectivity (and rain rate) is useful for retrieving rain rates from satellite radar measurements. Due to surface back scatter "leakage" into range gates close to the surface (range-time sidelobes), the retrieval algorithms need to extrapolate from aloft (around 2 km height) to surface level, or what is termed as "near surface rain rate". At present, the development of GPM retrieval algorithms for dual-wavelength radars is on-going, and in some cases, the algorithms require *a priori* constraints on the vertical covariances which need to be embedded in the algorithms in order to remove some of the unrealistic ambiguities that are present in the radar measurements (Tanelli, private communication).

This paper presents height-correlations of radar reflectivity determined from a zenith-pointing S-band radar in Singapore. The radar was deployed in early 1998 and was operational for 4 years (Thurai et al., 2003). Figure 1 shows the radar location. Disdrometers, rain gauges, and several other instrumentations were also collocated at the radar site. From the recorded events, several examples of stratiform and convective events have been chosen to determine the height correlations of radar reflectivity and rainfall rates, the latter using the appropriate Z-R relationships determined from a collocated JWD disdrometer.

2. INSTRUMENTATION AND DATA

An overview of the radar hardware can be found in Thurai et al., (2003), and details of a similar system which was deployed in another tropical location can be found in Eastment et al., (1998).

*Corresponding author: M. Thurai, Dept. of ECE, Colorado State University, Fort Collins, CO 80523. email: merhala@engr.colostate,edu

The radar uses a 3 m-diameter dish antenna equipped with a dual-polarization (horizontal and vertical) feed. The antenna has a gain of 36.5 dBi, a 3- dB beamwidth of 2.3°, and an integrated cross-polar isolation of around –25 dB. The transmitter uses a magnetron of 600 kW peak output power, operating at 3028 MHz. The radar operates at a PRF of 625 Hz with a pulse-length of 0.5 μs. The ADC bank samples co- and cross-polar log video, co-polar I and Q, transmit-pulse I and Q, and transmitted power at a rate of 2 MHz. Transmitted polarization is always horizontal, with simultaneous reception of horizontally and vertically polarized returns. The above parameters result in a maximum unambiguous range of 240 km, a maximum unambiguous velocity of around 15.5 m/s, and a range-resolution of 75 m. Data were generally recorded with an instrumented range of 0 to 45 km, and the number of pulses used is 64 or 256 in the vertically-pointing mode. *The unique feature of these operating parameters is that a vertical profile of data is acquired in 0.1-0.4 s (as compared with VHF/UHF profilers which can take up to several minutes). Thus very high resolution is obtained both temporally and spatially, and in particular, for computing the vertical correlations of Z (Section 4).* The Z, LDR, Doppler mean velocity (v) and spectral width (w) are recorded for each height-profile. Data from a collocated disdrometer (JWD) have been used to establish calibration as well as to determine suitable Z-R relations to determine rainfall rates from the radar measurements. (A comprehensive analysis of the disdrometer data has been published elsewhere, e.g. Kozu et al. 2006).

3. STRATIFROM AND CONVECTIVE EVENTS

An example of a stratiform event is shown in Fig. 2 and an example of a convective event, followed by 'mixed' and stratiform' rain is shown in Fig. 3. In both cases, the top 3 panels show the height versus time series color-filled plots for (a) Z, (b) LDR, and (c) v. The melting layer is clearly visible at around 4.5 km in all 3 plots in Fig. 2, and especially so in the LDR plot.

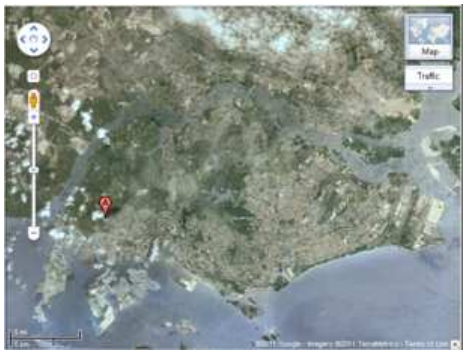

Fig. 1: Map showing the radar location (red mark).

The radar bright-band is also evident in Fig. 3, but only after 19:00. Between 19:30 and 20:30, the bright-band thickness is noticeably larger (than in Fig. 2(a)) as is its reflectivity values and its height appears to be somewhat lowered, as seen more clearly in LDR. The reflectivity in the rain region below is also larger, and LDR in rain appears to be detectable during this time period also. At some certain gates there appears clutter contamination (e.g. at around 3.5 km) perhaps due to near-by building scatter via the antenna sidelobes. The Doppler mean is particularly affected by such clutter (as expected).

The 1-minute DSDs from the disdrometer measurements were processed to calculate the S-band reflectivity at vertical incidence for an ambient temperature of 22 deg C. The calculations are compared with the radar-measured reflectivities at 1 and 2 km in panel (d) in Fig. (2) and (3). A finite calibration factor had to be added to the radar reflectivities in order to obtain the close agreement in both figures, and moreover time-shifts have been applied to the radar data to account for the drop fall velocities.

The disdrometer data were also used to determine the Z-R relations for the two events. Fig. 4 shows the plots, with the blue points corresponding to the stratiform rain period between 01:00 and 04:00 and the red points corresponding to the convective rain period between 17:00 and 18:00. The green line tracks the transition period from 18:00 all the way to 22:00, and as seen it largely lies within the boundaries set by the stratiform and the convective (blue and red) points. This trend has been observed in many prior studies (e.g. Tokay and Short, 1996).

The disdrometer data based Z-R relations for the two cases are included in the plot. Panel (e) in Fig (2) and (3) show the rain rates determined from the fitted equations and the radar reflectivities at 1 km and 2 km heights and compares with the disdrometer-data derived R. Once again close agreement is seen in both plots, and note the rain rate ranges from 0.5 mm/h up to nearly 100 mm/h. Finally the last panel (f) in Fig (2) and (3) show the 'stratiform-convective index' as was defined in an earlier study (Bringi et al., 2009, equations (6) and (7)) in Darwin, Australia, which had shown a clear separation in the N_W-D_0 domain. The same equation has been applied to the Singapore data (disdrometer-based) and the resulting index shows the same trend, i.e. high positive values during the convective period, (17:00-18:00) largely negative values during stratiform rain period (01:00-04:00) and somewhat close to zero values during the transition or mixed period and the 'thicker bright-band' period (19:00-20:00).

The convective events in Singapore can be variable in intensity, and in Fig. 5 we show an example of a severe storm which reaches up to heights of 15 km agl. Note the different scales used for this case, and note also that the spectral width is included for this case. The storm has high up and down drafts and strong wind shears, as well as high spectral widths indicating strong turbulence. LDR values in some regions are as much as -10 dB with corresponding reflectivities exceeding 60 dBZ. In the next section, we compare the height correlations of the radar reflectivities and rain rates.

4. HEIGHT-CORRELATIONS

In the earlier publication (Thurai et al., 2003), height profiles of reflectivity relative to 4 km a.g.l. were determined from 8 months of data (e.g. the color panels of Fig. 4 in the reference). In this paper, we quantify the height variation in terms of the correlation between time series of reflectivity as well as rain rate estimates at varying heights. However, since the reflectivity time series (from which the rain rates are estimated) tend to be rather 'noisy', a 'Lee-type' filtering (see for example Lee, 1980) is used for smoothing the high time resolution data. The smoothed time series is converted to rainfall rates using the appropriate Z-R relations, which in turn are used to evaluate the Pearson correlation coefficient using the lowest height with non-clutter-contaminated data as the reference. The whole process is repeated for various heights above ground level, for the chosen events, both during straiform rain period and convective rain period. For convenience, a bulk categorization of rain-type is performed using 1-hour blocks.

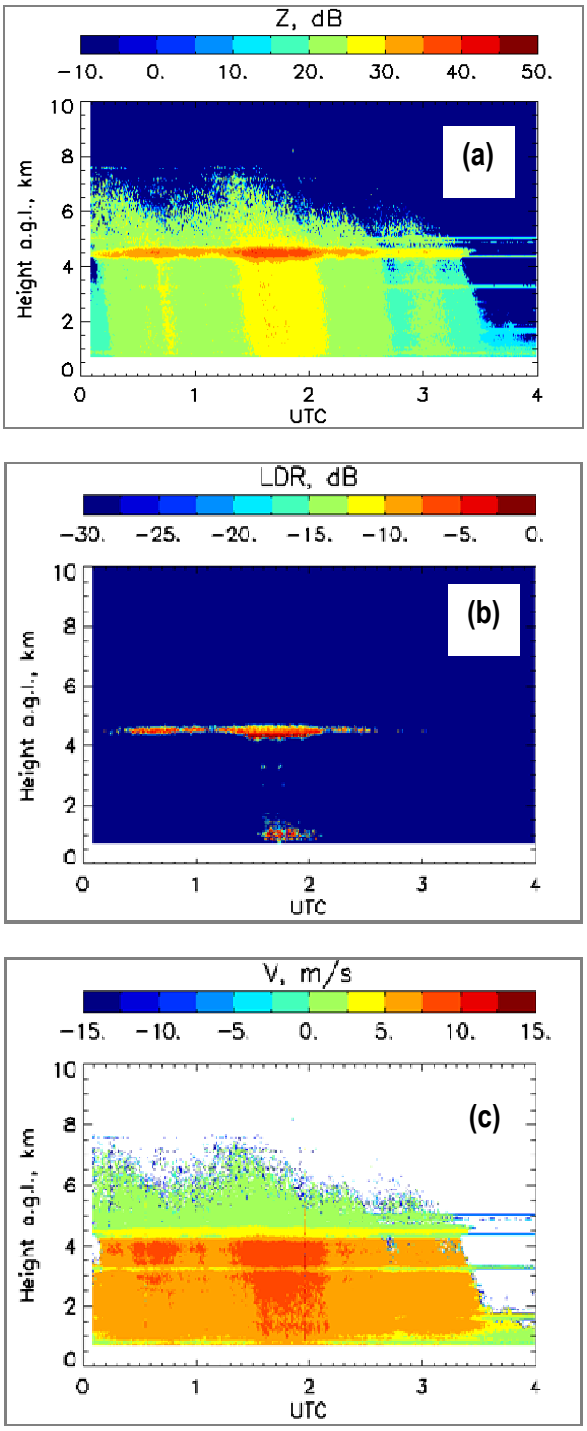

Fig. 2 : An example of a stratiform rain event. Height versus time series profiles of (a) radar reflectivity, (b) LDR, and (c) Doppler mean. (Day 363, 1998).

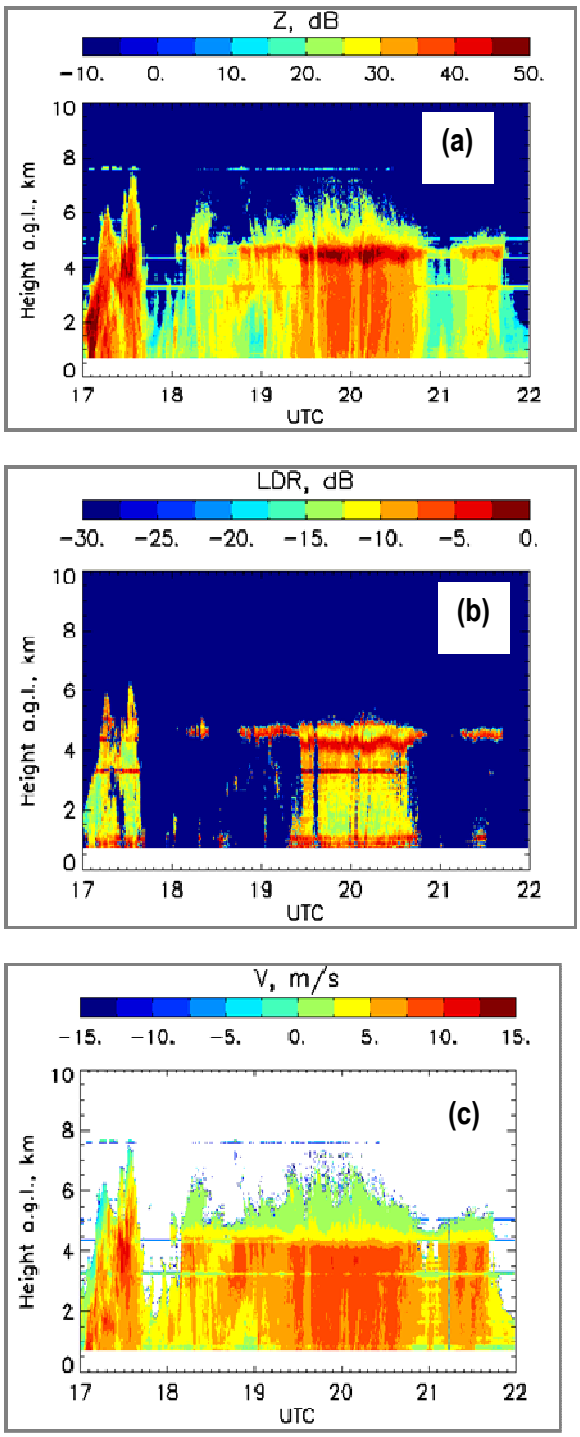

Fig 3: An example of a convective rain event, followed by mixed stratiform rain. Height versus time series profiles of (a) radar reflectivity, (b) LDR, and (c) Doppler mean. (Day 363, 1998).

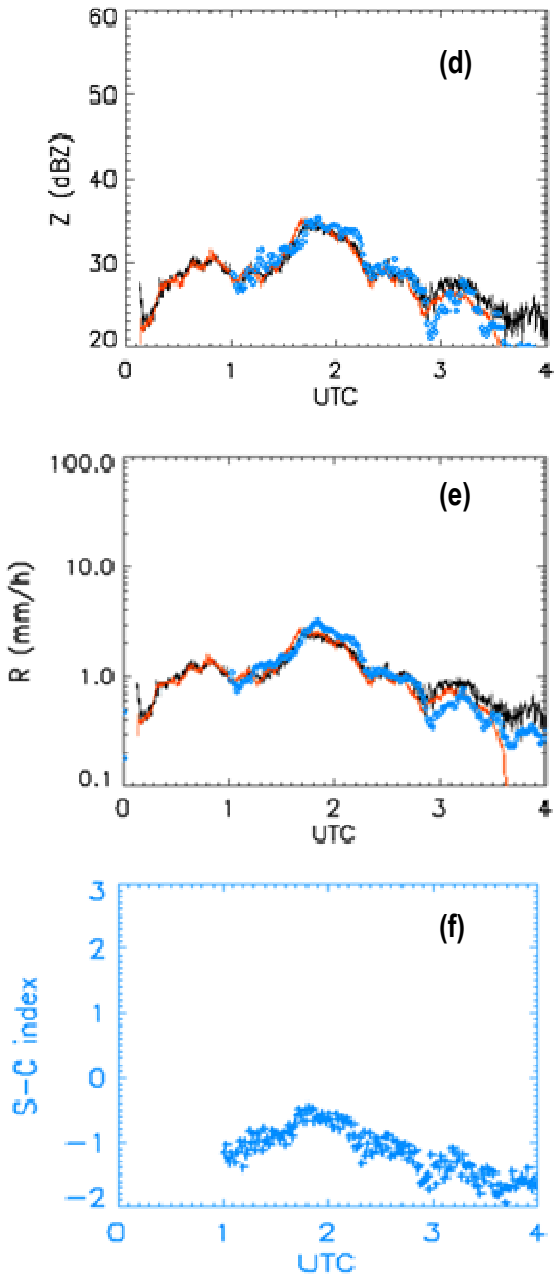

Fig. 2: (d) Disdrometer-based Z comparisons (blue) with radar measurements at 1 km (black) and 2 km (orange); (e) the corresponding rainrate comparisons; (f) the stratiform-convective index based on the 1-minute DSD from the disdrometer.

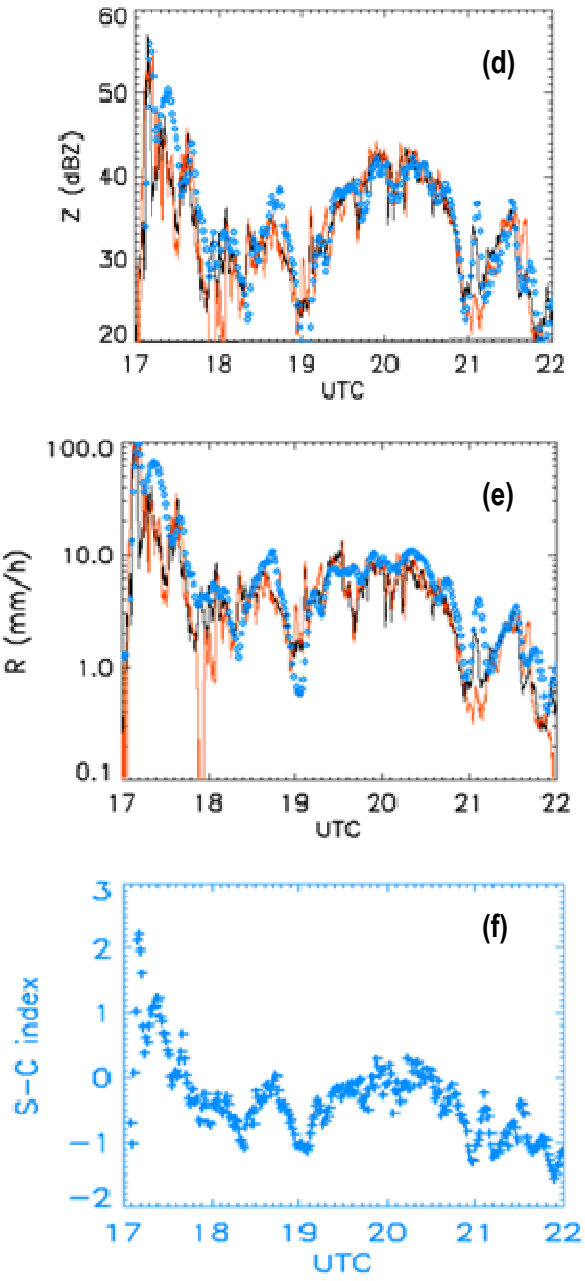

Fig 3: (d) Disdrometer-based Z comparisons (blue) with radar measurements at 1 km (black) and 2 km (orange); (e) the corresponding rainrate comparisons; (f) the stratiform-convective index based on the 1-minute DSD from the disdrometer.

The resulting correlations corresponding to the events in Fig (2) and (3) are given in Fig. 6(a) for the clear stratiform period (01:00 to 02:00 and 02:00 to 03:00) and for the convective period (17:00 to 18:00). The correlation curves will be the same for $\log_{10}$ R because of the power-law Z-R relationship. The two stratiform rain curves are close to each other whilst the convective rain case is distinctly different and falls faster than the other two, at least at heights below the nominal 0 deg C isotherm. Above 4 km, the stratiform rain curves (correlation values) rapidly decrease from 0.8 to 0.5 at 5 km due to the melting layer.

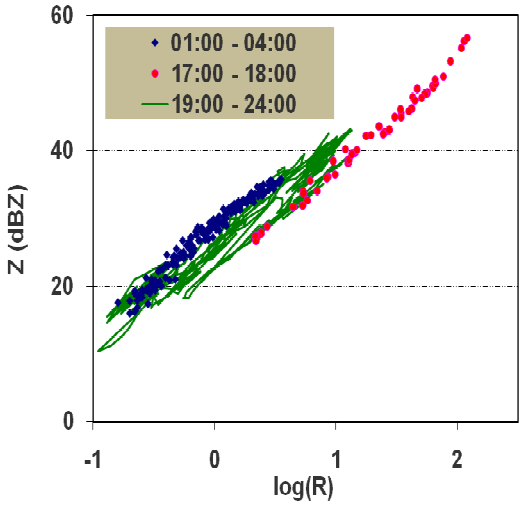

Fig. 4: Z-R relationships for the events shown in Fig. 2 (blue) and Fig 3, (red and green) using 1-minute DSDs. (all on day 363, 1998)

Fig. 6(b) shows the same three height profiles, and includes the corresponding profiles for two other cases, namely the intense storm in Fig. 5 (in yellow) and the strong stratiform rain period between 19:00 and 20:00 (in green) which had exhibited a much thicker bright-band. The former is somewhat close to the other convective rain case, although the rate of decrease at the lower heights is a little faster. The green curve lies in between the two sets of curves, implying perhaps that this case is not a steady stratifrom rain case (compared to 01:00-03:00 UTC). It would seem therefore that stratiform rain with a larger bright-band thickness may need to be considered different from the steady stratiform rain as far as vertical correlations are concerned (in addition to differences in the microphysics).

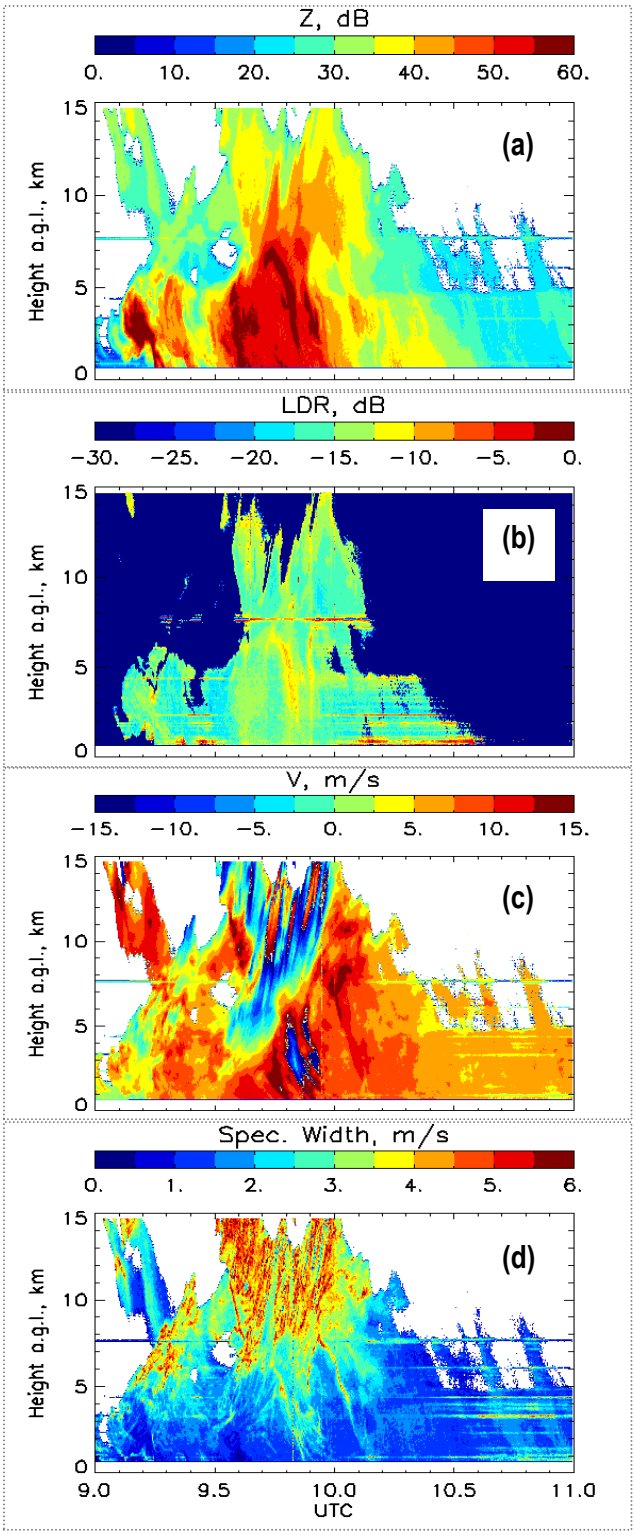

Fig. 5: A severe convective event: time series profiles of (a) Z , (b) LDR, (c) v, and (d) w (02 April 2001). Note the height and the intensity scales are different from Fig. 2 and 3.

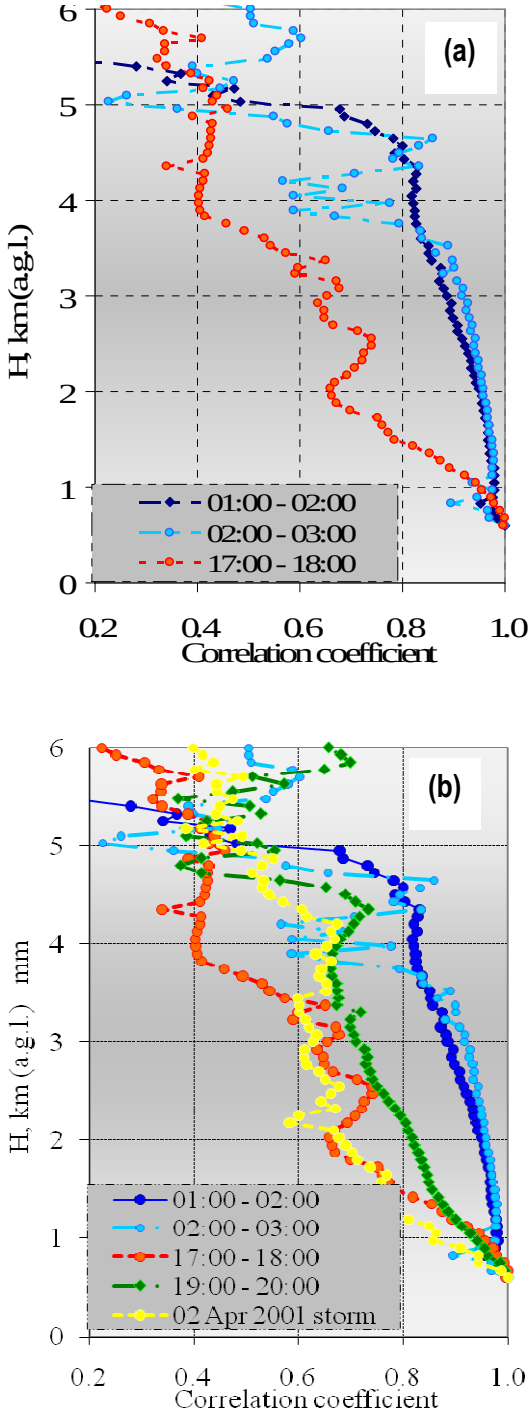

Fig. 6: (a) Correlation coefficient versus height a. g. l. for stratiform rain (light and dark blue curves) and for convective rain (red) corresponding to the time periods in Fig. 2 and 3 (both on day 363 of 1998); (b) two additional curves, one for the intense bright-band rain case (green) and one for the severe convective rain case (yellow) in Fig. 5 on 02 April 2001.

The vertical correlations of Z (in dBZ units) were fitted to a three-parameter exponential model given by:

$$\rho(d) = \rho_0 \exp\left[-(d / R_0)^F\right] \quad (1)$$

where d represents the separation distance, R_0 is the correlation radius, F is the shape parameter and ρ_0 is the nugget parameter (by definition equal to 1.0). The fitting was restricted to heights in the 0.6 to 3.0 km region except for the two convective cases which were restricted to 0.6 to 2.0 km (because the correlations at d > 2 km were too variable for obtaining a "good" fit). Table 1 compares the fitted coefficients with 0.6 km as the 'reference'. As with the height correlation curves in Fig 6, the fitted parameters in Table 1 will be the same for $\log_{10}$ R because of the power-law Z-R relationship.

TABLE 1: Fitted coefficients for the curves in Fig. 6 using equation (1)

Time period	Rain type	R_0 (km)	F	H_{max}
01:00 to 02:00	Stratiform	10.75	1.41	3 km
02:00 to 03:00	Stratiform	10.65	1.58	3 km
19:00 to 20:00	Thick bright-band case	8.6	0.86	3 km
17:00 to 18:00	Convective	5.2	0.88	2 km
02Apr 2001 09:30 to 10:00	Severe convection	9.8	0.8	2 km

The two stratiform rain cases have higher correlation radius values than the two convective cases (which is not unexpected) and their F values are sufficiently above 1 to give a convex shape near the reference height, whereas the convective cases show F values less than 1 (concave near the reference height). *We believe that this is a new finding as far as vertical correlation shape differences between stratiform and convective rain is concerned*. Note that the lowest F value is obtained for the very intense storm on 02

April 2001. The height correlation curve for this case and the curve for the (lighter) stratiform case (02:00-03:00) may be considered as the boundary limits for most rain events. Other 1-hour data-blocks extracted from the recorded datasets in Singapore can be used to investigate this further.

5. CONCLUSIONS

The vertical correlation of Z (in dBZ) has been determined at high temporal (5 second) and spatial resolutions (75 m) using a vertically pointing S-band radar. As expected, steady stratiform rain shows much slower decay in correlation (larger decorrelation distance) than convective events. A modified exponential fit with shape parameter *F* (eq. 1) shows a distinct difference in *F*, being significantly greater than 1 (1.4 - 1.6) resulting in a convex shape near s=0 for stratiform rain, whereas *F* is less than 1 (0.8 - 0.9, implying concave) for convective rain. A thick bright-band case shows a height correlation structure in-between the two. An exceptionally strong convective event shows the fastest decrease in correlation with height, reducing from 1 at 0.6 km to 0.66 at 2 km.

Acknowledgements: MT and VNB were supported by the NASA PMM science grant NNX10AJ11G.

REFERENCES

Bringi, V. N., C. R. Williams, M. Thurai, P. T. May, 2009: Using Dual-Polarized Radar and Dual-Frequency Profiler for DSD Characterization: A Case Study from Darwin, Australia. J. Atmos. Oceanic Technol., 26, 2107–2122.

Eastment, J. D., M. Thurai, D. N. Ladd, and I. N. Moore, 1998: Radiowave propagation research in the tropics using a transportable multiparameter radar system, Electronics & Communication Engineering Journal, Feb 1998, 4-16, doi: 10.1049/ecej:19980102

Kozu, T., K. K. Reddy, S. Mori, M. Thurai, J. T. Ong, D. N. Rao and T. Shimomai, 2006: Seasonal and Diurnal Variations of Raindrop Size Distribution in Asian Monsoon Region, Journal of the Meteorological Society of Japan, Vol. 84A (special issue),195-209,

Lee, J. S., 1980: Digital image enhancement and noise filtering by use of local statistics, IEEE Trans. Pattern Analysis Machine Intell., PAMI-2(2), 165–168.

Thurai, M., T. Iguchi, T. Kozu, J. D. Eastment, C. L. Wilson, and J. T. Ong, 2003: Radar observations in Singapore and their implications for TRMM Precipitation radar retrieval algorithms, Radio Science, 38 (5), doi:10.1029/2002RS002855.

Tokay, A., and D. A. Short, 1996: Evidence from tropical raindrop spectra of the origin of rain from stratiform versus convective clouds. J. Appl. Meteor., 35, 355–371.